Vortex-Generating Coolant-Flow-Passage Design for Increased Film-Cooling Effectiveness and Surface Coverage

S. Stephen Papell

NASA

Vortex-Generating Coolant-Flow-Passage Design for Increased Film-Cooling Effectiveness and Surface Coverage

S. Stephen Papell
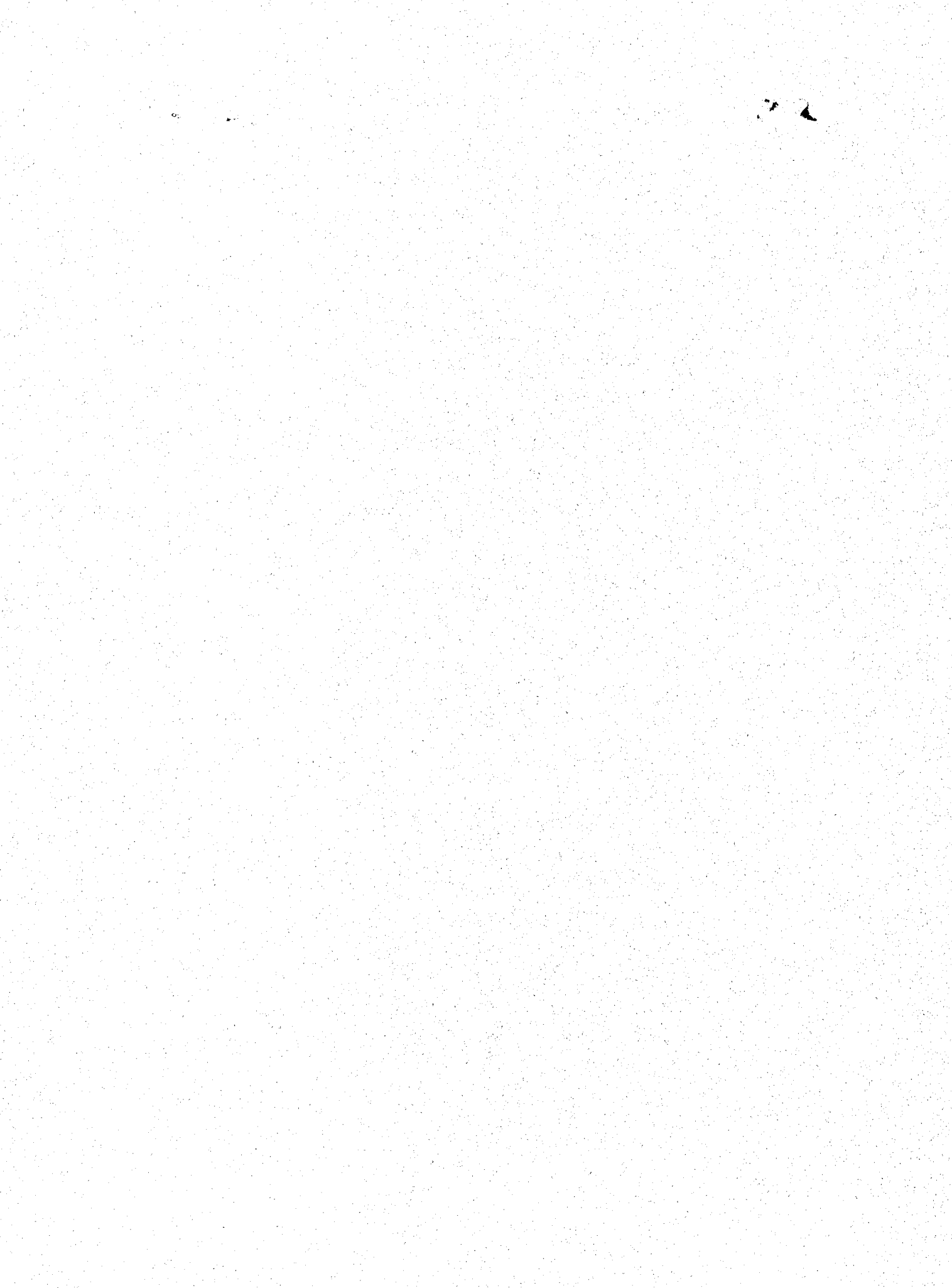
Lewis Research Center
Cleveland, Ohio

Summary

The study used an inclined jet in crossflow as a model to aid in the development of the hypothesis that a coolant-channel contour could increase film-cooling efficiency. The coolant channel, by virtue of its shape, generated a counterrotating vortex pair secondary flow within the coolant flow. The interaction of the vortex structure generated by the flow passage and the vortex structure generated by the mainstream and boundary flow was examined in terms of film-cooling effectiveness and surface coverage.

Reported herein are the thermal film-cooling footprints observed by infrared imagery for three coolant-passage configurations embedded in adiabatic test plates. A round-hole cross section was used as a reference with which to compare the performance of two orientations of the new, vortex-generating flow passage. For both orientations the vortex-generating coolant passages showed up to factors of four increases in both film-cooling effectiveness and surface coverage over that obtained with the round coolant passage. The crossflow data covered a range of tunnel velocities from 15.5 to 45 m/sec with blowing rates from 0.20 to 2.05.

In addition, it was determined that flow separation of an inclined jet from the surface containing the hole configuration could be inhibited by a coolant-passage geometry that generates a counterrotating vortex pair structure in the coolant flow that rotates in opposition to the vortex pair rotation generated by the crossflow.

A photographic streakline flow visualization technique was used that supported the concept of the counterrotating capability of the flow passage design and gave visual credence to the explanation offered for the differences found in the data.

Introduction

Film cooling is well established as a viable method for protecting turbine blades and vanes in high-performance engines for advanced aircraft. Since the coolant itself is drawn from compressor pressurized air that is part of the aerodynamic cycle of the engine, it becomes necessary to use it as efficiently as possible.

In actual use the coolant enters the base of the blading and is ejected through holes drilled at some angle through the blading surfaces. Although the coolant passages are generally straight with a circular cross section, some attempts have been made to increase the effectiveness of the film-cooling process by design modifications. Engine manufacturing companies are working to develop inlet and exit passage contouring techniques with encouraging results. References 1 and 2, in which the influence of coolant-passage curvature on film cooling was examined, report that curvature increases the effectiveness of film-cooling by about 35 percent at the low blowing rates but that at higher blowing rates curvature decreases the effectiveness.

The present study uses an inclined jet in crossflow as a model to hypothesize a coolant-channel contour that increases the effectiveness of film-cooling. The design concept requires that the coolant channel generate a counterrotating vortex pair secondary flow within the coolant jet by virtue of the shape of the flow channel. The interaction of the vortex structure generated by the flow passage and that generated by the crossflow was examined in terms of film-cooling effectiveness and surface area coverage. Comparative data obtained with a round coolant passage were used to evaluate the worth of this new design concept.

Reported herein are the thermal film-cooling footprints obtained by infrared imagery for the vortex-generating and the round coolant passages embedded at an angle of 30° in adiabatic test plates. The crossflow covered a range of velocities from 15.5 to 45.0 m/sec with blowing rates from 0.20 to 2.05. Temperature differences between the coolant and crossflow was about 22° C.

Symbols

C centrifugal force

D drag

d coolant-tube diameter

M blowing rate, $(\rho V)_c/(\rho V)_\infty$

m momentum change

R radius

T	temperature
t	adiabatic plate thickness
u	crossflow velocity
V	velocity
x	distance from downstream edge of coolant port to downstream edge of isotherm trace
x/d	dimensionless distance
η	adiabatic film-cooling effectiveness, $(T_\infty - T_{aw})/(T_\infty - T_c)$
ρ	density

Subscripts:

aw	adiabatic wall
c	coolant
j	jet
∞	free stream or tunnel air

Fluid Dynamic Modeling

Inclined Jet in Crossflow

The film-cooling mechanism is the injection of a cool film of air into a boundary layer to provide an insulating layer between a hot gas and metal surfaces. For the protection of turbine blading the coolant is ejected through discrete holes drilled at some angle in the blade wall so that the basic fluid dynamic process is essentially an inclined jet in crossflow. The literature contains many studies relating to the mixing process associated with a jet in crossflow (e.g., refs. 3 and 4).

Figure 1 is a schematic of an inclined jet in crossflow showing the forces on a control element of the jet. The drag D acts opposite to the direction of the relative velocity caused by the interaction of the crossflow velocity V_∞ and the jet velocity V_c. The centrifugal force C is normal to the jet path, and the momentum change m acts along the jet path.

There are three well-defined turbulent mixing processes associated with this momentum change that contribute to the breakup of the jet. The first is the mixing that occurs along the interface between the jet and the crossflow. The second is just downstream of the jet exit port where a pressure rarefaction pulls the tunnel air sideways under and into the jet stream. The third mixing process occurs within the jet stream itself with the formation of a vortex structure (schematically illustrated in fig. 2) as a counter-rotating vortex pair. The vortex strength and the distance between vortex centers, which influence the width of the jet, are also functions of the crossflow momentum. The cross section of the jet (fig. 2) shows that the direction of rotation for this vortex pair structure is down on the sides

and up through the center. This direction of rotation, induced by the crossflow is quite significant and will be further discussed later.

From this simple model it is evident that the discrete-hole film-cooling process is controlled by the energy available in the crossflow. It is suggested that this energy is distributed in a manner to influence the jet trajectory, the three turbulent mixing processes described above, and the spreading of the jet on the surface to be protected.

The design concept was to modify the coolant-jet stream by inducing a vortex structure within the coolant flow, similar to that shown in figure 2, by virtue of the shape of the coolant passage. It was postulated that this geometry-induced vorticity could replace the crossflow energy required to generate the vortex flow structure within the jet and, as a result, make available more crossflow energy to turn the jet closer to the wall and/or increase the vortex strength to spread the jet. Both of these flow mechanisms should increase the effectiveness of the film-cooling process.

It was also suggested that the direction of rotation of the counterrotating vortex structure generated by the passage geometry could be reversed with respect to the crossflow generated vortex structure. In this manner both vortex structures would tend to cancel each other at the coolant-injection port. If this were possible, the mixing that occurs due to the tunnel air being pulled sideways and under the jet stream could be prevented or minimized.

Coolant Passage Design Concept

The vortex-generating coolant flow passage design concept is illustrated in figure 3 along with a round coolant flow passage for comparison. The cross section of the vortex-generating passage in figure 3(a) is somewhat elliptical, with a flat surface on one of the long ends of the ellipse and a cusp surface on the opposite end. Figure 3(b) shows the edge of cusp extending along the length of the flow passage that provides the vortex-generating capability of the coolant passage.

The double curved surfaces of the cusp should split the flow into two streams that rotate in opposite directions, producing a vortex pair structure within the coolant stream. Within the passage the direction of this vortex pair rotation is from the center of the flat surface (fig. 3(a)) toward the cusp edge and out along the curved surfaces in opposite directions. The direction of this geometry-induced rotation with respect to the crossflow, therefore, depends on the orientation of the cusp edge in the flow passage. Figure 4 illustrates the two cusp orientations used in this study. With the cusp surface on the top of the jet stream (fig. 4(a)), the direction of rotation is upward toward the cusp edge and down on the sides. With the cusp surface at the bottom of the jet stream (fig.

2

4(b)), the rotation is downward toward the cusp edge and upward along the sides.

It, therefore, follows from figure 4 that the vortex structure generated by the top-cusp geometry enhances the vortex structure generated by the crossflow by rotating in the same direction, while that generated by the bottom-cusp geometry tends to cancel the crossflow-generated vortex structure. The interactions of these sets of vortex pairs and their influence on film-cooling efficiency is the subject of this study.

Apparatus

The actual coolant passage design used is illustrated in figure 5, which also shows the dimensions of the coolant passages. Both the round and vortex-generating passages were cast in epoxy as inserts to be installed in the flat plate shown in figure 6. The round passage had a flow diameter of 1.27 cm; the contoured vortex-generating passage was sized to have the same flow area. Thus, for the same mass flow, the discharge velocity of the coolant was the same. Both passages discharged the coolant at an angle of 30° to the surface in line with the tunnel flow.

The test plate was made of mahogany with a thickness of 6.35 cm that minimized heat transfer through its wall. In addition, the thick plate also provided a ratio of thickness to coolant-passage effective diameter t/d of 5, which is typical of holes drilled in the walls of cooled turbine blading. The coolant-passage inserts were hand fitted to an opening in the test plate designed to accept them. The surfaces of the plate and the passage inserts were finished smooth and painted a uniform dull black to increase their radiation emissivity. The top of the plenum (fig. 6) was attached to the bottom of the test plate. The coolant air supplied to the plenum entered the coolant passage at very low velocity. The plenum assembly contained a system of baffles and screens and was covered with fiberglass insulation.

The test plate and plenum assembly were installed as part of the tunnel floor shown in figure 7. The tunnel itself, designed for flow visualization, was made of clear plastic sections with a flow area cross section of 15 by 38 cm. A contoured inlet and a transition piece connected to the altitude exhaust system of the laboratory completed the tunnel assembly.

The tunnel section containing the test plate was positioned so that there was 1.3 m of tunnel length (not including the contoured inlet) in front of the coolant-injection port. In a previous investigation (ref. 2) velocity profiles were obtained in this tunnel by both hot-wire and Pitot tube probes. These measurements assured the establishment of fully developed turbulent flow at the coolant-injection port. Under the flow conditions of this study the tunnel flow boundary layer thickness was about 1.65 cm, and the turbulence intensity of the free stream was about 3 percent.

The coolant was supplied to the plenum by use of a Hilsch tube connected to a 8.3-kPa (120-psi) dry air source. This source, which incorporates a vortex-generator element, separates the inlet air into hot and cold streams. This results from the forced vortex or wheel type of angular velocity imparted to the air entering the device. Conservation of the total energy of the inner portion of the contained vortex causes heat to be transferred to the outer region of the vortex. Consequently, a relatively cold inner core of air and a warm outer ring of air are available. In the Hilsch tube design the warm and cold air discharge ports are on opposite ends of the tube. Cold side temperatures of 0° C are available with this device so that temperature differences between the tunnel and coolant airflow of about 22° C could be readily obtained.

The tunnel air temperature was measured with a thermocouple mounted in the contoured inlet. The coolant-air temperature was measured with a thermocouple mounted in the plenum between the screens and the mahogany test plate. The coolant airflow rate was measured with a turbine type flowmeter installed between the Hilsch tube and the coolant plenum.

The infrared camera and detector unit used to measure the surface temperature downstream of the coolant-injection port was capable of operating within the temperature range of -30° to 200° C and could discriminate temperature differences as small as 0.2° C. The detector element was indium antinomide cooled by a liquid-nitrogen bath. The detector displayed the isotherm image on the cathode-ray screen, from which it was then photographed for a permanent record. A reference isotherm at a known temperature was obtained for each data run by focusing the camera on the test plate at a position not influenced by the cooling air jet. The temperature at this position was measured with thermocouples embedded in the plate.

Examples of photographic data are shown in figure 8, which presents equal temperature isotherm traces of the round and cusped coolant channels for data obtained at identical test conditions. The temperatures of the isotherm traces are indicated in thermal scale units by the tick marks along the abscissa on the photographs. The comparison of these scale readings previously described permit the evaluation of the isotherm temperatures. The two vertical lines on the photographs are the field-of-view limits of the infrared detector. These lines are centered so that the left line abuts the downstream edge of the coolant-injection port, which is not shown in the photograph.

Experimental Procedure and Data Reduction

The experimental data obtained for this study enabled the evaluation of film-cooling effectiveness and surface area coverage for each isotherm trace. The controlled parameters for these tests were tunnel air velocity (crossflow), coolant velocity, and coolant temperature. The coolant temperature, measured in the plenum, was set near 0° C by controlling the Hilsch tube valves. The tunnel air temperature, depending on ambient conditions, was about 25° C. Variations in the blowing rate were obtained by control of tunnel and Hilsch tube airflow valve settings.

The testing procedure required an initial cool down of the plenum before a desired blowing rate was set. The temperatures were then allowed to come to equilibrium before data collection commenced. Eight infrared photographs were taken for each test setting that covered the temperature range of the film-cooling footprint. The testing procedure was repeated over a range of tunnel velocity settings and blowing rates for all coolant passages studied.

The film-cooling effectiveness of each isotherm trace was calculated as

$$\eta = \frac{T_\infty - T_{aw}}{T_\infty - T_c} \tag{1}$$

where T_∞, T_c, and T_{aw} are temperatures of the tunnel air, coolant, and plate, respectively. Information gained from these traces also included interpretations of isotherm shapes with regard to the mixing processes of both air streams. For example, the photographs in figure 8 illustrate the differences in isotherm traces obtained under the same test conditions for the round and top-cusp coolant-passage geometries. The differences in size and shape of the traces are readily observed. The round coolant passage trace (fig. 8(a)) closes on itself at the end nearer to the coolant-injection port. Since the plate surface temperature outside of the enclosed trace is warmer than the trace itself, the warmer plate temperature near the coolant-injection port suggests that the jet did not attach to the surface until some distance downstream. The pressure rarefaction that occurs just downstream of the injection port due to the passage angularity with respect to the tunnel flow is responsible for this flow separation phenomena.

Two types of measurements were obtained from the infrared photographs. The first was the centerline length of each isotherm trace measured from the downstream edge of the coolant-injection port to the downstream edge of the trace. The second measurement, performed with a planometer, was the surface area enclosed by the trace.

The results of this investigation, presented graphically, covered data obtained at specific test conditions of tunnel velocity 15.5, 22.8, 30.5, and 45.0 m/s and blowing rates from 0.20 to 2.05 for each of the three coolant-passage geometries.

Presentation of Data and Flow Phenomena

Centerline Film Cooling Effectiveness (Basic Data)

Distributions of film-cooling effectiveness downstream of the coolant-injection port are presented in figures 9 to 11 for the round, top-cusp, and bottom-cusp coolant passages. The data are plotted as film-cooling effectiveness as a function of dimensionless distance (x/d) along the centerline from the edge of the coolant-injection port. The round coolant passage data (fig. 9) show an expected trend that is influenced by tunnel velocity and blowing rate. An increase in tunnel velocity generally increases the level of each curve for a constant blowing rate. For a constant tunnel velocity an increase in blowing rate first increases the level of the curves up to about $M = 0.50$, and then decreases the level of the curves as the blowing rate increases.

The distance downstream of the injection port for maximum effectiveness depends on the blowing rate. Figure 9(a) shows that at $M = 0.20$ the maximization of each curve occurs at the coolant-injection port, suggesting an immediate attachment of the jet stream to the plate. With increasing blowing rate the maximization of each curve shifts downstream from about 2 hole diameters at $M = 0.34$ to 6 hole diameters at $M = 2.05$.

This position shift in maximum effectiveness is caused by flow separation of the jet due to the angularity of the coolant passage with respect to the crossflow. It is suggested that maximization occurs where the energy in the crossflow forces the jet stream to attach to the plate surface.

The individual curves plotted in figure 9 were obtained from lines drawn through data points as shown in figure 9(c), which is representative of the extent of the scatter in the data. At the higher blowing rates (figs. 9(f) to (h)), rig limitations in the availability of the coolant flow rates through the Hilsch tube did not permit covering the full range of tunnel velocity data.

The top-cusp film-cooling effectiveness data obtained under the same test conditions as the round coolant passage data are shown in figure 10. The tunnel velocity and blowing rate trends are similar to those obtained with the round coolant passage (fig. 9). In addition, the profiles of the curves are also similar, including the shift in maximum effectiveness due to the delayed jet stream attachment phenomena described above.

The bottom-cusp data obtained under the same test conditions are shown in figure 11. The tunnel velocity and blowing rate trends are similar to those obtained with the other coolant-passage geometries, but the position of maximum effectiveness and the shapes of the data curves are quite different.

An examination of the eight sets of data in figure 11 shows that for all blowing rates the position of maximum effectiveness occurs at the coolant-injection port. Apparently, the vortex-generated flow due to the bottom-cusp geometry did not permit jet separation under any blowing rate.

The shapes of the effectiveness profiles shown in figure 11 are functions of the blowing rates. At the lowest blowing rate ($M = 0.20$) the shapes of the curves are similar to those of figures 9 and 10. At higher blowing rates ($M = 0.34$ and 0.50; figs. 9(b) and (c)) the horizontal dashed lines indicate a flattening of the profiles within 4 diameter downstream of the port, depending on the tunnel air velocity. At the higher blowing rates ($M = 1.00$ to 2.05; figs. 9(e) to (h)) the shapes of the curves presented change significantly. An inflection appears in the data profiles at a position downstream of the coolant-injection port between x/d values of 4 to 5.

An explanation for this unique inflection that appears in the effectiveness profiles for the bottom-cusp data lies in the direction of vortex pair rotation induced by the coolant-passage geometry, which in this orientation is opposite to the rotation induced by the crossflow. Within 4 to 5 diameters of the coolant exit, the geometry-induced vortex flow structure predominates but is finally overcome by the crossflow induced vortex flow further downstream.

Data Comparisons

Differences in centerline film-cooling effectiveness performance of the round, top- and bottom-cusp coolant passages are illustrated in figures 12 to 15. Each figure presents data for a constant value of tunnel velocity over a range of blowing rates. The individual curves, plotted as film-cooling effectiveness against hole diameters downstream from the edge of the coolant port, were obtained from the basic data presented in figures 9 to 11. The trends that appear in the comparative data plots of the figures are quite similar for all four sets of data.

In all cases the film-cooling performance of the round cross section passage was inferior to that of the new, vortex-generating passage in either cusp orientation. For dimensionless distances (x/d) greater than 4, the data trends are quite regular. The top-cusp coolant-passage data show the highest film-cooling effectiveness, and the round coolant passage data shows the lowest. The bottom-cusp data fall in between, with its position relative to the top-cusp and round coolant passage data a function of blowing rate. At low blowing rates the

bottom-cusp data fall close to the round coolant passage data but, as the blowing rate increased, shift closer to the top-cusp data.

For dimensionless distances (x/d) less than 4, which is close to the coolant-injection port, a reversal occurs in the relationship between the cusp orientations and the vortex-generating passage, with the bottom-cusp passage becoming more effective. The effectiveness differences increases considerably at the higher blowing rates.

The general results drawn from the data of figures 12 to 15 is that the top-cusp coolant-passage is superior in performance to both the bottom-cusp and the round coolant passage configurations except for close to the coolant-injection port, where, at $M \geq 1.00$, the bottom-cusp passage becomes superior. Differences in the data up to a factor of 4 in film-cooling effectiveness can be readily obtained by choice of coolant-passage geometry.

Film Cooling Coverage (Basic Data)

The surface areas enclosed by the isotherm traces were obtained from the infrared photographs and plotted in terms of film-cooling effectiveness based on the measured adiabatic temperatures of the isotherms. The data curves are presented in figures 16 to 18 for the three coolant passage geometries. The individual curves were obtained from lines drawn through data points as shown in figure 16(b), which is representative of the scatter in the data.

An examination of the three sets of data shows similar trends, which are also influenced by tunnel velocities and blowing rates. Increasing tunnel velocity generally increases the level of each curve for a constant blowing rate, while increasing blowing rates first increases then decreases the level of the curves. In general, the curves of figures 16 to 18 show a maximization of film-cooling effectiveness occurring at the lowest values of isotherm area coverage with a gradual reduction in effectiveness with increasing area coverage.

Data Comparison

Differences in film-cooling effectiveness as a function of isotherm area coverage for the three coolant-passage geometries are illustrated in figures 19 to 22. The curves were obtained from the basic data in figures 16 to 18. Each figure presents data for a constant value of tunnel velocity over a range of blowing rates.

The trends illustrated in figure 19 for a tunnel velocity of 15.5 m/s show the superior performance of the top-cusp passage over the round passage for the entire range of blowing rates from ($M = 0.20$ to 2.05); the bottom-cusp curves lie between these two sets of curves in a position that depends on the blowing rate. At the lowest blowing rate ($M = 0.20$; fig. 19(a)) the bottom-cusp data fall on or close to the round coolant passage data. With increasing blowing rate, the bottom-cusp curve shifts in

5

the direction of the top-cusp curve, and at $M=2.05$ the curves are quite close to each other. These same data trends are repeated in figures 20 to 22 for tunnel velocities of $V_\infty=22.5$, 30.5, and 45.0 m/s.

In general it appears that, for a constant value of film-cooling effectiveness, the coolant flow from the top-cusp passage covers a larger surface area than is available from the round coolant passage. In addition, the area covered with coolant flow from the bottom-cusp passage falls between the other two passages in a position that depends on the blowing rates. Differences in surface area coverage under the same flow conditions of up to a factor of 4 can be readily obtained by choice of coolant-passage geometry.

Discussion

The improved film-cooling performance of the vortex-generating coolant passage over the round-cross-section passage has been demonstrated herein for the range of blowing rates relevant to turbine blade cooling ($M=0.20$ to 2.05). The evidence is graphically presented in plots obtained under identical test conditions. It was determined that the coolant passage, by virtue of its geometry, generates a counterrotating vortex pair structure within the coolant flow that is similar to the vortex structure generated by the crossflow. The cusp surface coolant-passage design evolved along with the following arguments. Because the cusped surface in the coolant passage controls the vortex pair direction of rotation, it was believed that a change in rotation direction could be achieved by orienting the cusp surface on the top or at the bottom of the jet stream. It was also believed that this difference in induced vortex rotation would influence the data. The vortex structure generated by the top-cusp geometry enhanced the vortex structure generated by the crossflow because they rotate in the same directions. The vortex structure generated by the bottom-cusp geometry rotates in opposite the directions and tends to cancel the vortex structure of the crossflow. The fluid dynamic interactions of these sets of vortex pairs were used to explain the differences in the data.

There are separate arguments that apply to the different orientations of the cusp-shaped coolant passage. When the cusp surface in the passage is on top of the jet stream, both geometry and crossflow induced vortex rotations are in the same direction. For this orientation it was hypothesized that, when the flow is discharged into the tunnel mainstream, the geometry-induced vortices are already present and do not require initiation by the main stream. Consequently, the mainstream has more momentum available to turn the jet closer to the wall, resulting in enhanced film-cooling effectiveness.

When the cusp surface is oriented on the bottom of the jet stream, both vortex structures rotate in opposite directions and influence the jet separation phenomena previously described. Both the round and top-cusp coolant passages allow flow separation to occur due to a pressure rarefaction that occurs just downstream of the injection port. The flow separation results in a side flow pumping of the tunnel air under and into the jet stream. The direction of vortex pair rotation with the passage in the bottom-cusp orientation must therefore be responsible for preventing or minimizing this pumping from occurring.

Although significant isotherm data difference measurements obtained with the round, top- and bottom-cusp coolant passages could be attributed to geometric differences, the counterrotating pair vortex-generating capability of the cusp shaped passage could only be speculated. Therefore, a flow visualization study was conducted to attempt to visually establish the expected vorticity in the flow. A streakline flow visualization technique (ref. 5) was used to photograph very small, neutrally buoyant, helium-filled soap bubbles, about 1 mm in diameter, that followed the flow field. With a camera shutter speed of 12 frames per second, the bubble appears as a streak line on the film. The bubble generator outlet probe was set up to discharge into the coolant plenum thereby seeding the coolant flow. The indication of vorticity in the flow is then captured on film and can be identified by the twisting motions of the streaklines.

The photographs in figure 23 were obtained using a telephoto lens on a camera facing downstream from the tunnel inlet toward the front edge of the test plate. The horizontal white lines in these photographs are the surface of the test plate illuminated by the lamp that defines the exit of the coolant passage. In the absence of tunnel flow, a streakline rises from the the top-cusp passage toward the top of the tunnel (fig. 23(a)). The camera caught the bubble streak after it had emerged from the passage. Since there is no crossflow, vorticity must have been generated by the geometry of the coolant passage.

Figures 23(b) and (c) were obtained under conditions of crossflow with both the top- and bottom-cusp passages subjected to a blowing rate of 0.34 but at different tunnel flow rates. The crossflow momentum appears to have turned the coolant jet toward the surface away from the camera. The streak lines that appear to be moving into the paper reveal the twisting motion of the jet as it emerges from the edge of the coolant passage indicating vorticity. The counterrotating vorticity in the flow is also supported by these photographs in which the streak lines appear to be rotating in opposite directions. The division of flow appears quite clear; unfortunately the sense of rotation direction for the individual streams can only be speculated.

One of the speculations that could be proven by photography is the change in the trajectory of the jet stream caused by differences in coolant-passage geometry. This was accomplished by photographing from the side edge of the test plate. Figure 24 shows a streak line emerging from top-cusp passage with no crossflow. The jet flow ejects from the passage at an angle of 30° with respect to the plate surface. The pointer on the transparent wall of the tunnel is located at the downstream edge of the ejection port and establishes a reference measurement position. A bolt through the test plate and the edge of the tunnel wall serves as a reference position for measuring the height of the stream line at a fixed position downstream from the coolant-injection port. As did figure 23(a), figure 24 shows that the vorticity appearing in the streak line could be attributed to the cusp passage geometry.

The change in trajectory of the jet stream caused by differences in passage geometry, under identical flow conditions, is illustrated in figure 25. The jet trajectory from the round passage (fig. 25(a)) is significantly higher (farther from the reference bolt) than the trajectories from the top- and bottom-cusped passages (figs. 25(b) and (c)). The reason for the inferior film-cooling performance of the round jet passage (see figs. 12(f) and 19(f)) is revealed by these differences in trajectory shown in figure 25.

Summary of Results

The film-cooling isotherm data reported herein were obtained by infrared photography along with an apparatus designed to determine the film-cooling performance of three descrete-hole coolant-flow passages. The passages were embedded in adiabatic test plates and discharged the flow at an angle of 30° in line with the tunnel flow. The standard round hole cross section coolant passages was used as a reference with which to compare the performance of two orientations of a counterrotating vortex-pair generating coolant passage that evolved from an examination of the basic fluid dynamics of an inclined jet in crossflow.

Test conditions included blowing rates from 0.20 to 2.05 and tunnel velocities from 15.5 to 45.0 m/s, with temperature differences of about 22° C between the tunnel and coolant-air streams. Data comparisons are presented graphically as film-cooling effectiveness in terms of the centerline length of the isotherm traces measured from the edge of the coolant-injection port and also the surface area enclosed by the isotherm.

Interactions of the vortex pair structure in the coolant flow generated by passage geometry with the vortex pair generated by the crossflow was influenced the film-cooling process. Data obtained under the same test conditions showed up to factors of 4 increases in both centerline film-cooling effectiveness and surface area coverage over that obtained with the round cross section passage. In addition, flow separation of an inclined jet from the surface containing the passage could be depressed by a coolant-passage geometry that generates a counterrotating vortex pair structure within the coolant flow which rotates in opposition to the crossflow-generated vortex pair rotation.

A streak line flow visualization technique was used to support the concept of the counterrotating capability of the cusp-faced flow passage design. Photographic data showed the coolant flow split into two streams that rotate in opposite directions. In addition, the streak line trajectory from the round passage was considerably higher than from either the top- or bottom-cusp passages, attesting to differences obtained in the film-cooling data.

References

1. Papell, S.S.; Graham, R.W.; and Cageao, R.P.: Influence of Coolant Tube Curvature on Film Cooling Effectiveness as Detected by Infrared Imagery. NASA TP–1546, 1979.
2. Papell, S.S.; Wang, C.R.; and Graham, R.W.: Film-Cooling Effectiveness With Developing Coolant Flow Through Straight and Curved Tubular Passages. NASA TP–2062, 1982.
3. Abramovich, G.N.: The Theory of Turbulent Jets. M.I.T. Press, 1963.
4. Keffer, J.F.; and Baines, W.D.: The Round Turbulent Jet in a Cross Wind, J. Fluid Mech., vol. 15, pt. 4, Apr. 1963, pp. 481–496.
5. Colladay, R.S.; and Russell, L.M.: Streakline Flow Visualization of Discrete-Hole Film Cooling With Normal, Slanted, and Compound Angle Injection. NASA TN D–8248, 1976.
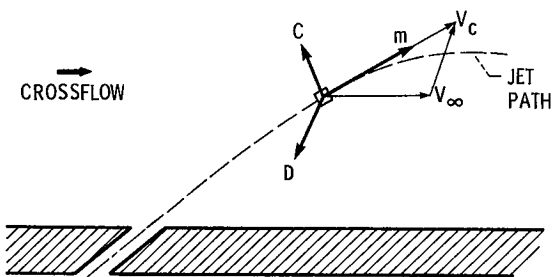
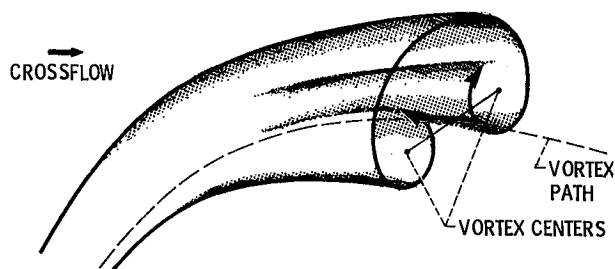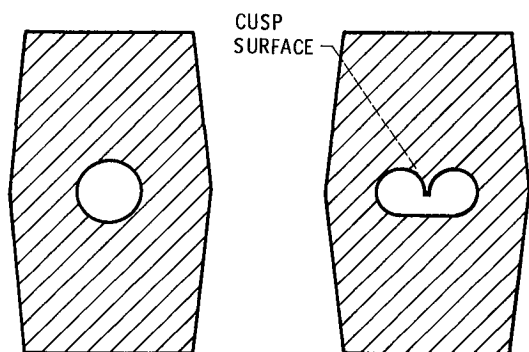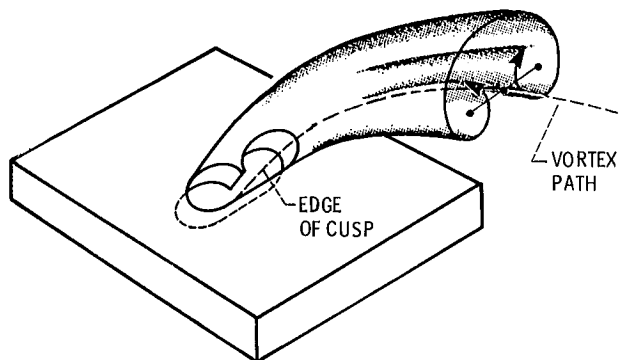Figure 1.—Inclined jet in crossflow showing forces on a control element.

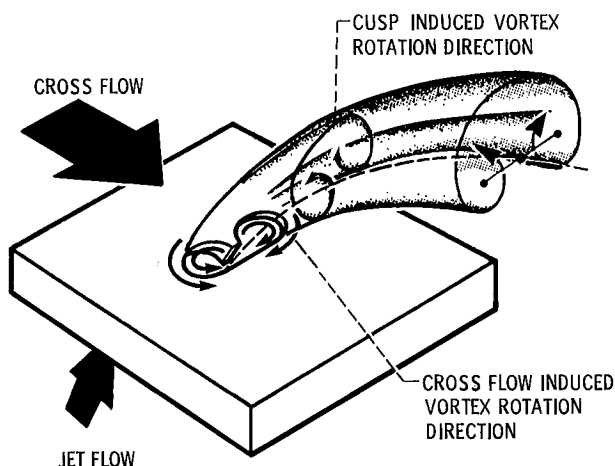Figure 2.—Counterrotating vortex pair structure within the jet induced by the crossflow.

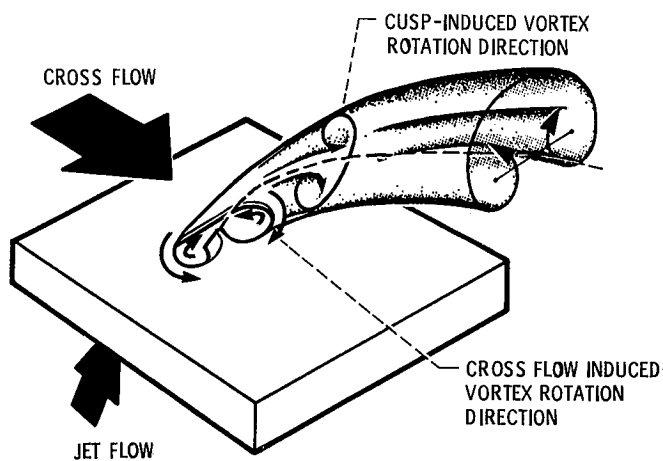(a) Coolant flow passage cross sections.
(b) Counterrotating vortex-generating coolant passage.

Figure 3.—Design concept.

(a) Top cusp orientation.
(b) Bottom cusp orientation.

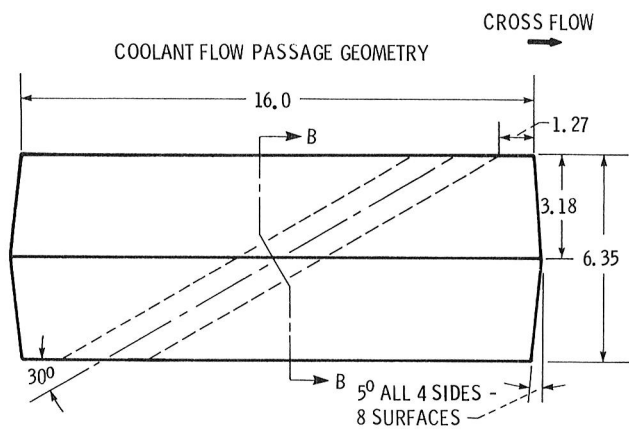Figure 4.—Geometry-induced vortex pairs with respect to crossflow-induced vortex rotation.

COOLANT FLOW PASSAGE GEOMETRY

CROSS FLOW

16.0

1.27

3.18

6.35

B

B

30°

5° ALL 4 SIDES –
8 SURFACES –

Figure 6.—Test plate and coolant-supply plenum.

TUNNEL
FLOW

CAST EPOXY
INSERT

MAHOGANY

30°

TEST PLATE

6.35 cm

SCREENS

BAFFLES

INSULATED
PLENUM WALL

COOLANT
SUPPLY

L

L/2

L/2

1.268
1.273 DIAM.

0.433 RAD.
0.436

0.025

BB – 1
ROUND

BB – 2
CUSP

Figure 5.—Design details of passage cross sections. (All dimensions in centimeters.)

TUNNEL FLOW

EDGE OF
HOLE

(a)

EDGE OF
HOLE

(b)
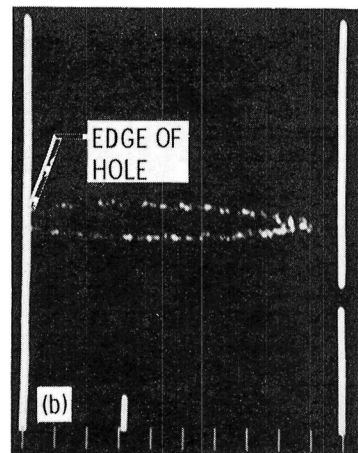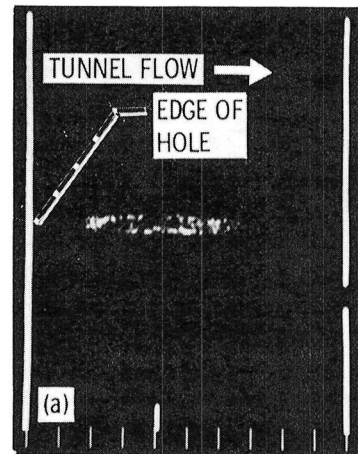
(a) Round.   (b) Top cusp.

Figure 8.—Equal temperature isotherm traces. Infrared photographs obtained under same test conditions. Tunnel velocity, V, 15.5 m/s; blowing rate, M, 1.00; film cooling effectiveness, η, 0.16.

INFRARED
CAMERA

OSCILLOSOCOPE
DISPLAY UNIT

THIN FILM
WINDOW

ADIABATIC
WALL

ALTITUDE
EXHAUST

ROOM
AIR

HOT
AIR

TUNNEL

PLENUM

COLD AIR

HILSCH
TUBE

TURBINE TYPE
OF FLOWMETER

AIR SUPPLY,
83 kPa (120 psi)
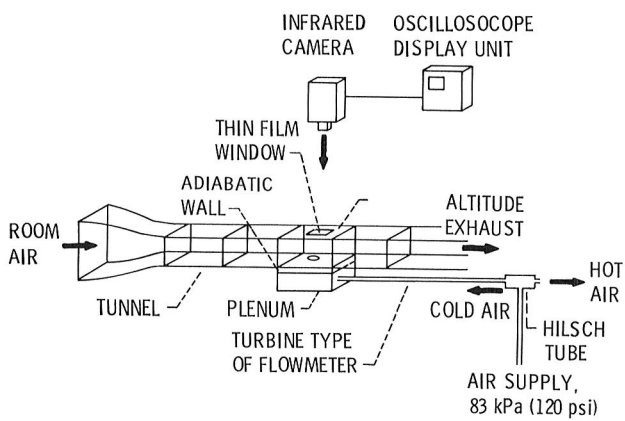
Figure 7.—Film-cooling rig.
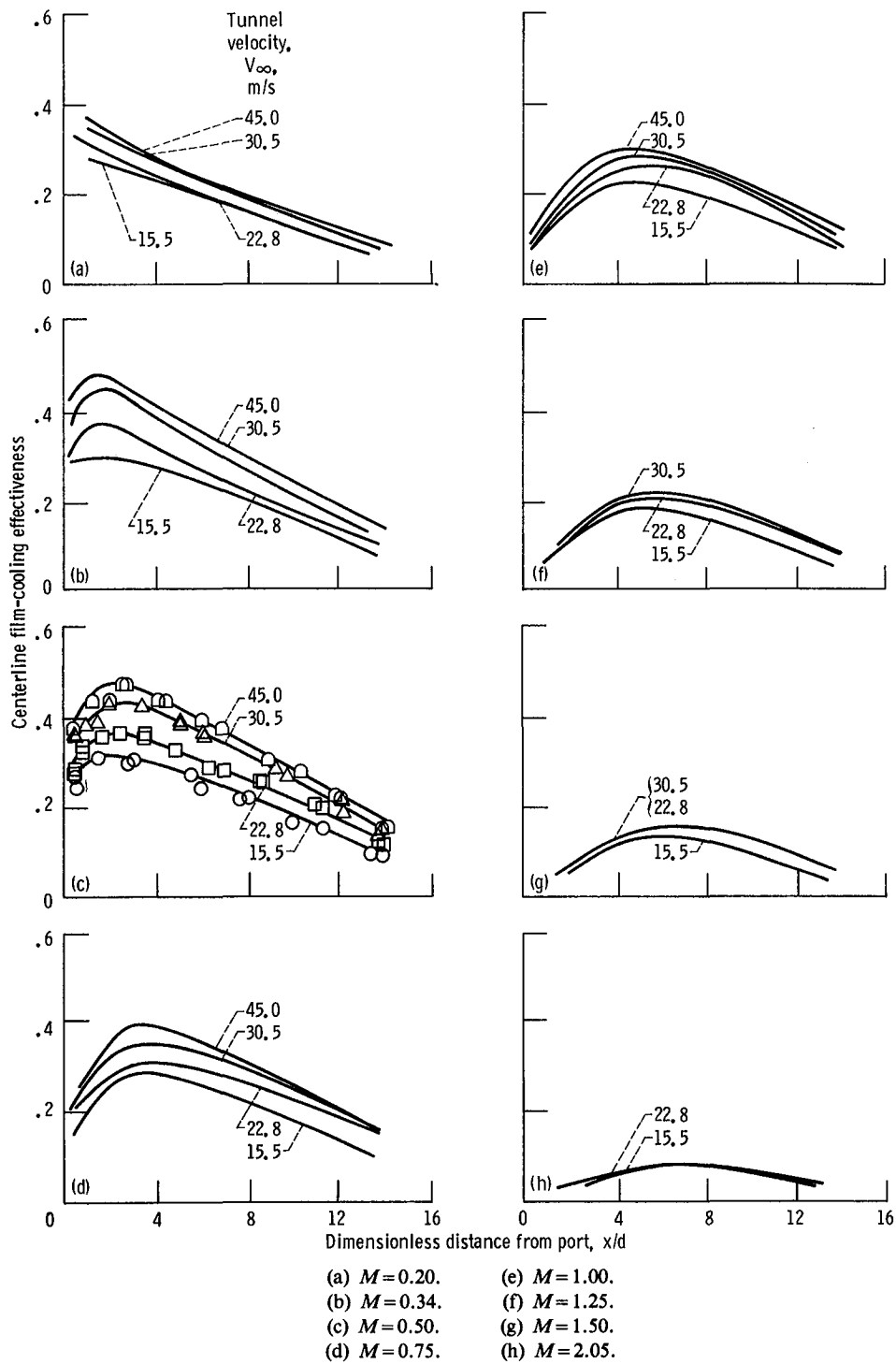
Figure 9.—Basic round coolant passage data.

(a) $M = 0.20$. (e) $M = 1.00$.
(b) $M = 0.34$. (f) $M = 1.25$.
(c) $M = 0.50$. (g) $M = 1.50$.
(d) $M = 0.75$. (h) $M = 2.05$.
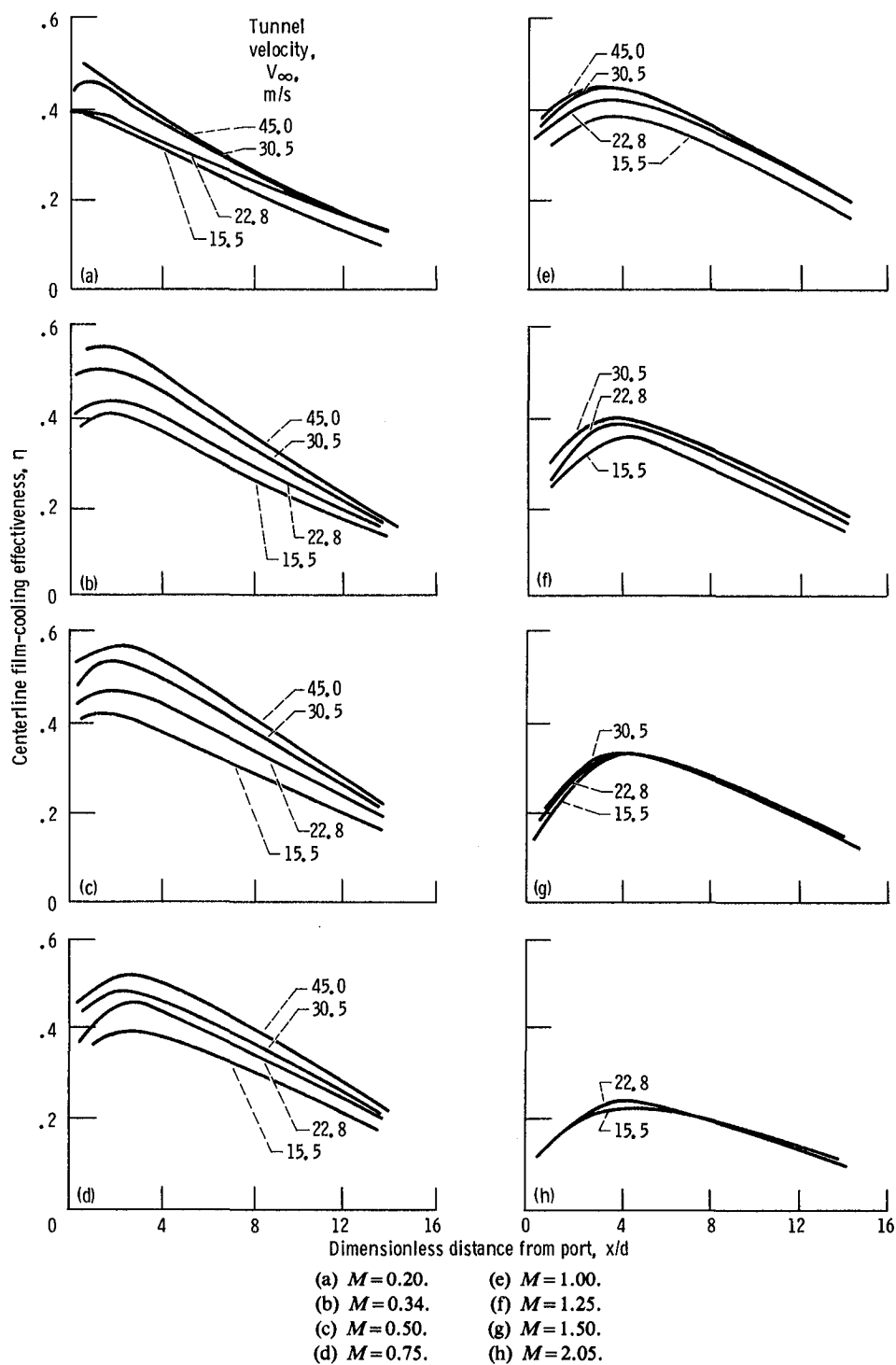
Figure 10.—Basic top-cusp coolant passage data.

(a) $M = 0.20$.   (e) $M = 1.00$.
(b) $M = 0.34$.   (f) $M = 1.25$.
(c) $M = 0.50$.   (g) $M = 1.50$.
(d) $M = 0.75$.   (h) $M = 2.05$.
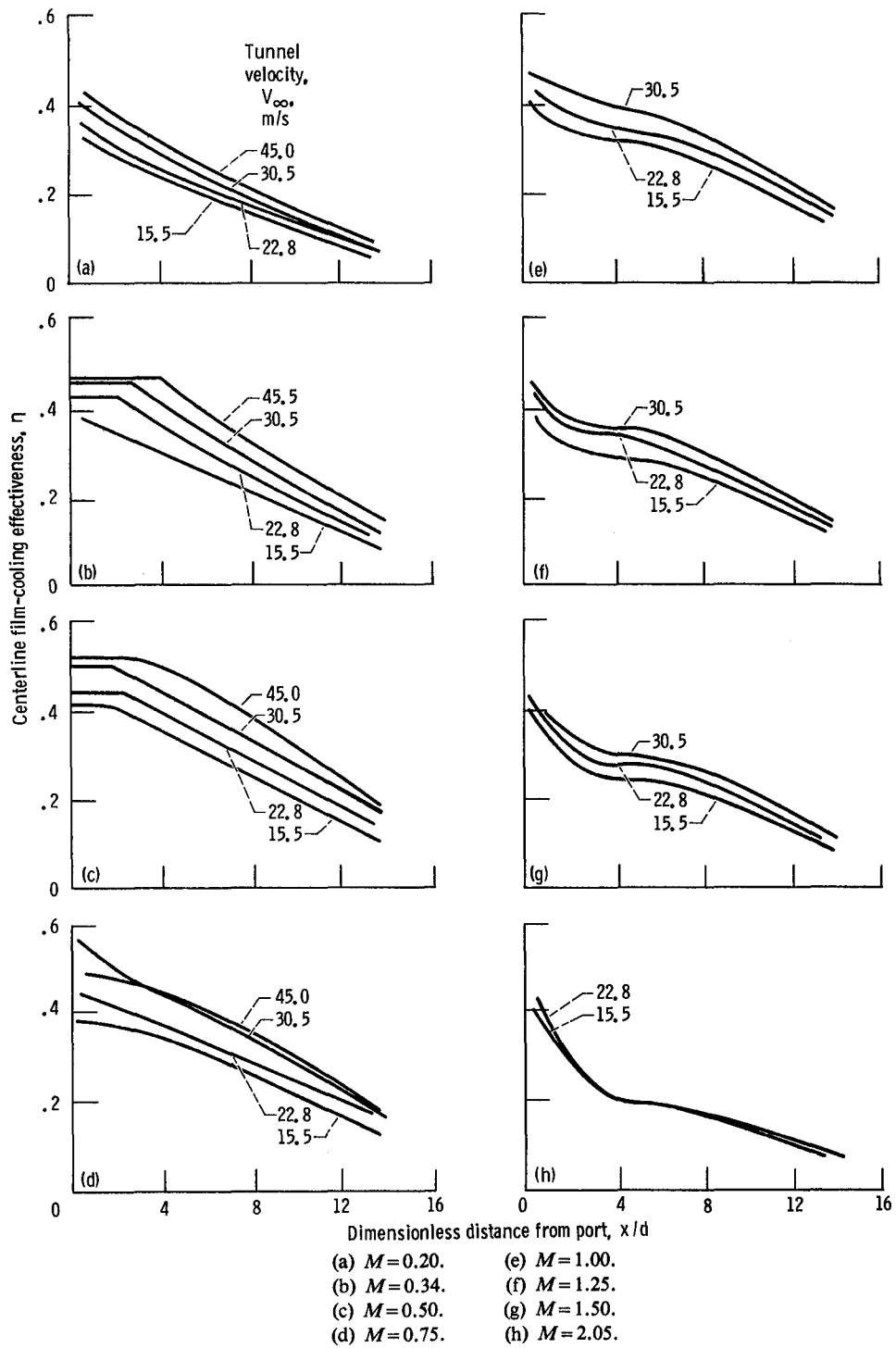
Figure 11.—Basic bottom-cusp coolant passage data.

(a) $M = 0.20$. (e) $M = 1.00$.
(b) $M = 0.34$. (f) $M = 1.25$.
(c) $M = 0.50$. (g) $M = 1.50$.
(d) $M = 0.75$. (h) $M = 2.05$.
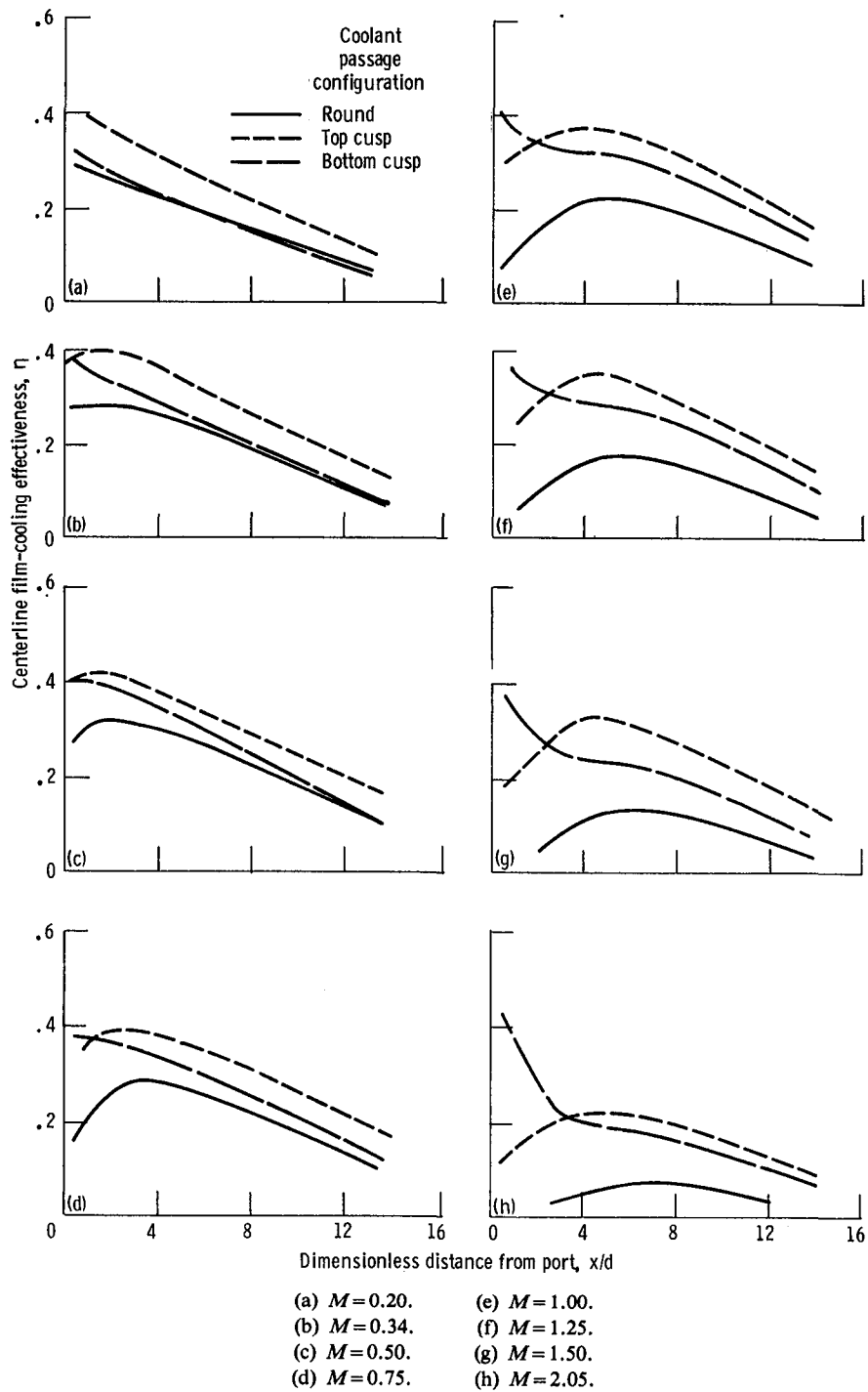
Figure 12.—Comparison of centerline film-cooling effectiveness distributions for free stream velocity of 15.5 m/s.
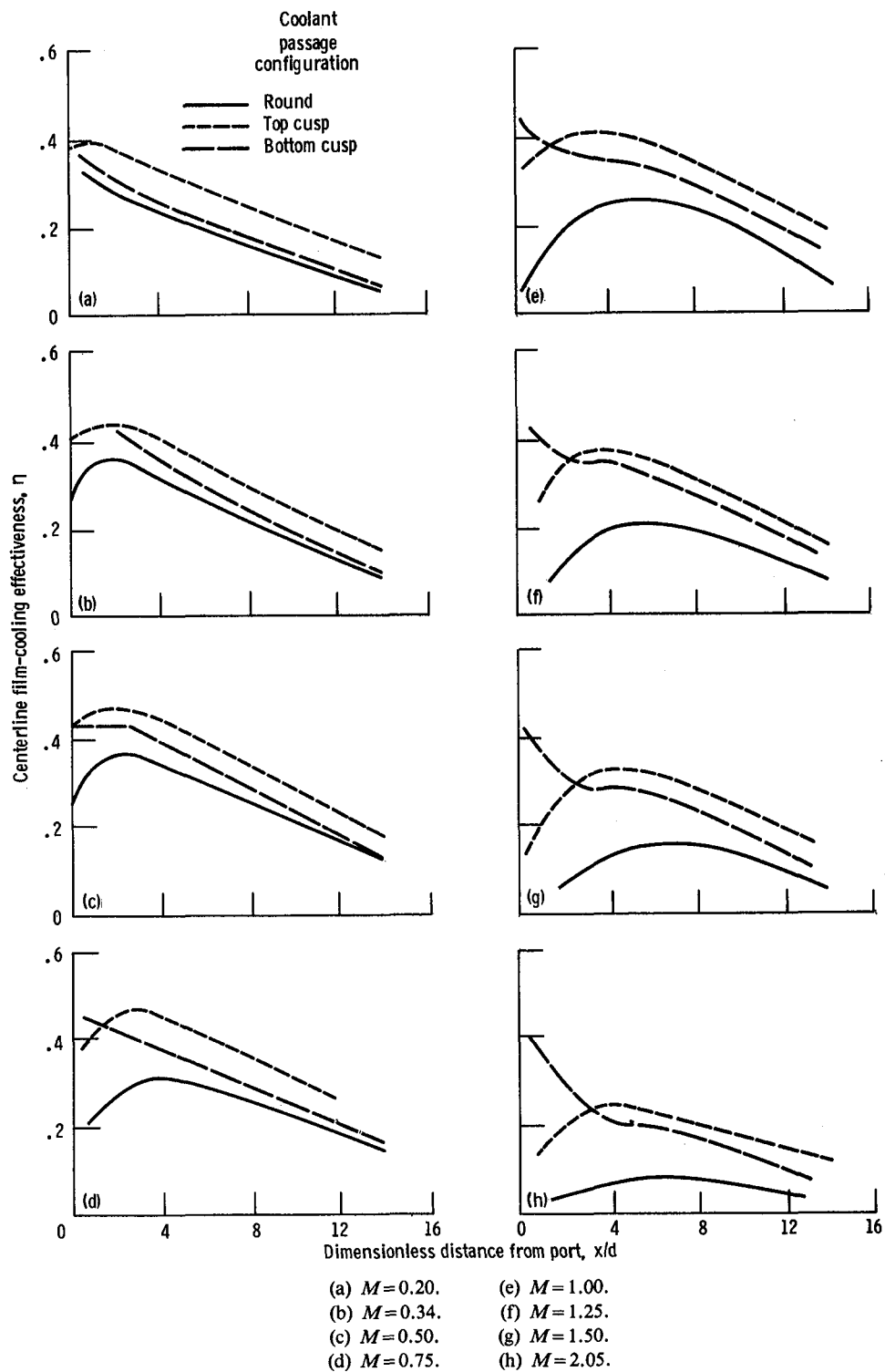
Figure 13.—Comparison of centerline film-cooling effectiveness distributions for free-stream velocity of 22.8 m/s.

(a) $M = 0.20$.   (e) $M = 1.00$.
(b) $M = 0.34$.   (f) $M = 1.25$.
(c) $M = 0.50$.   (g) $M = 1.50$.
(d) $M = 0.75$.   (h) $M = 2.05$.
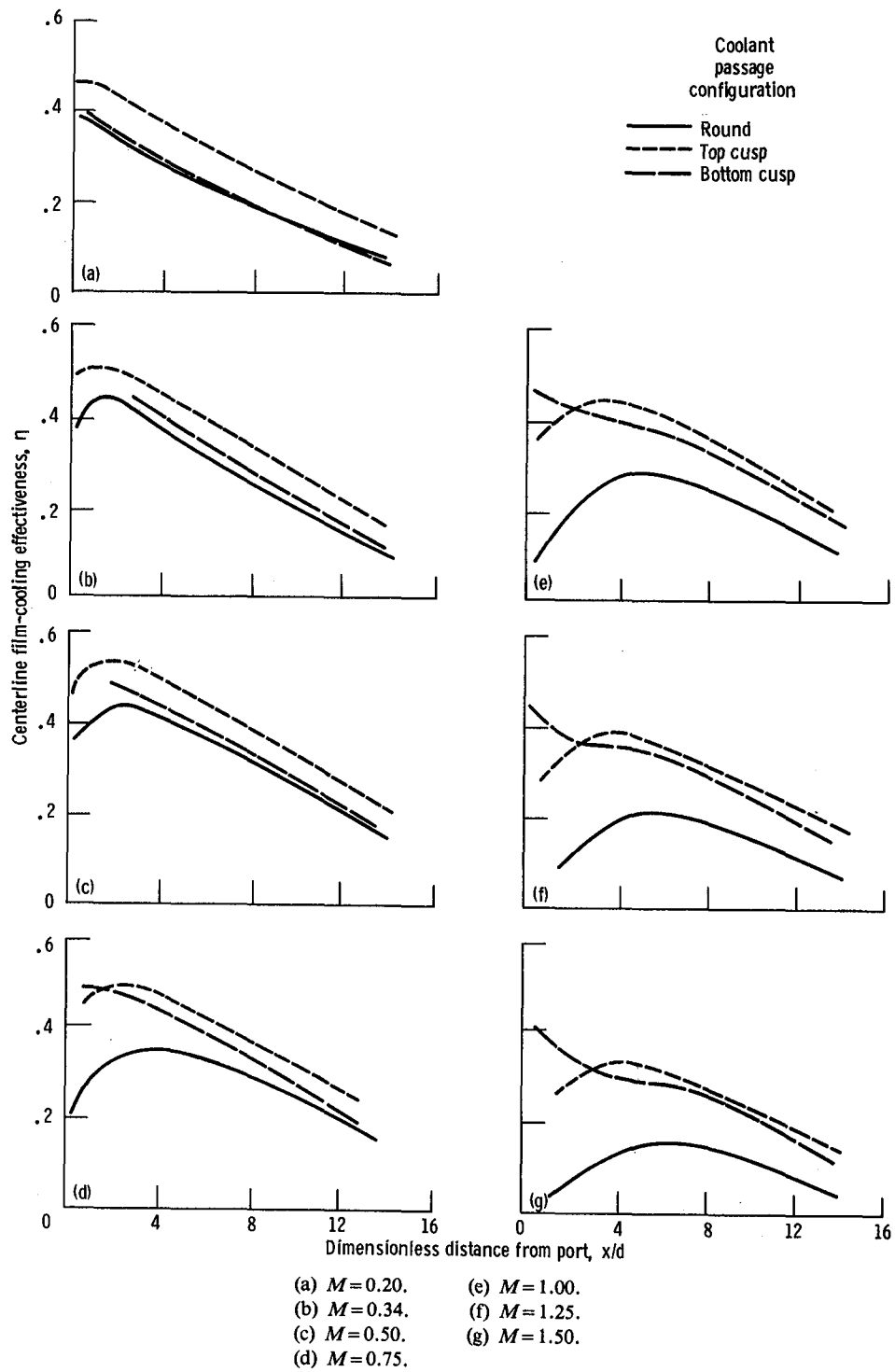
Figure 14.—Comparison of centerline film-cooling effectiveness distributions for free-stream velocity of 30.5 m/s.

(a) $M = 0.20$.   (e) $M = 1.00$.
(b) $M = 0.34$.   (f) $M = 1.25$.
(c) $M = 0.50$.   (g) $M = 1.50$.
(d) $M = 0.75$.
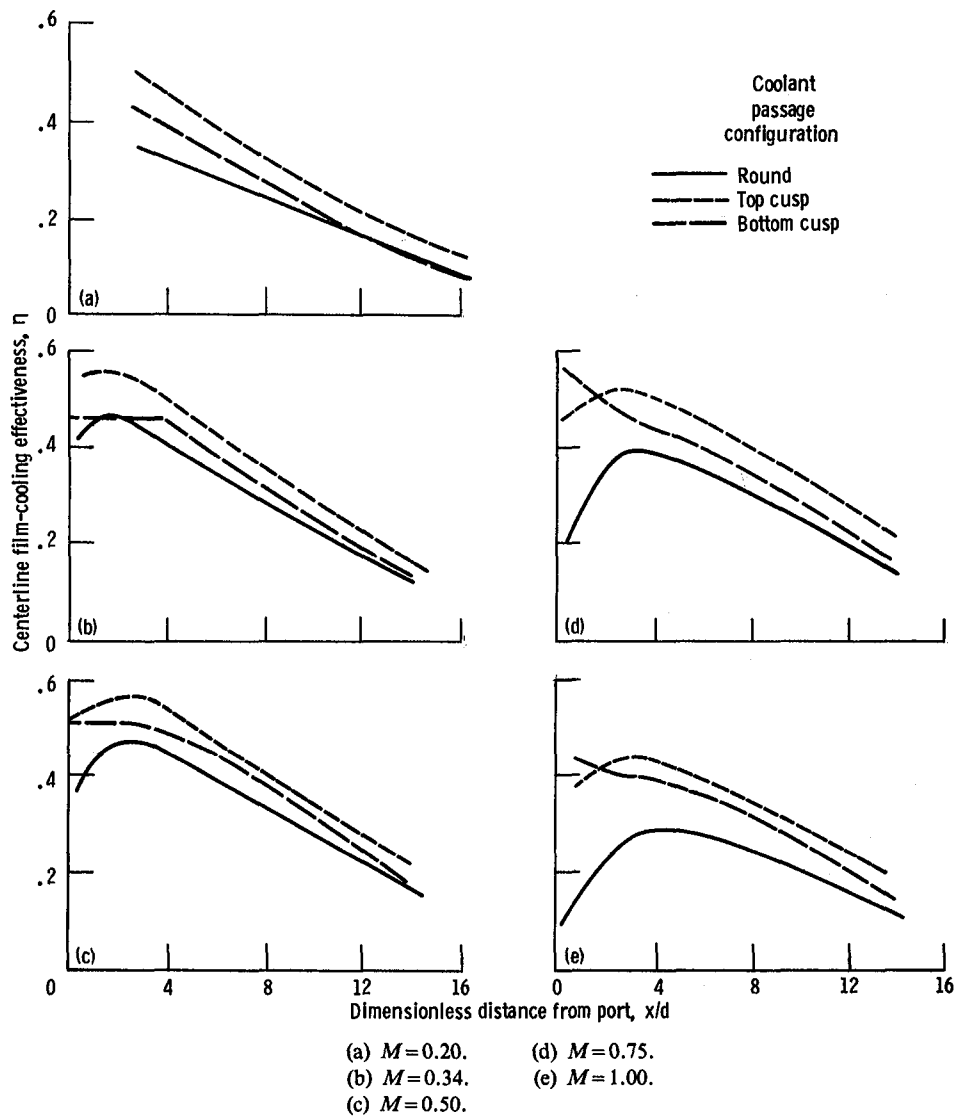
Figure 15.—Comparison of centerline film-cooling effectiveness distributions for free-stream velocity of 45.0 m/s.
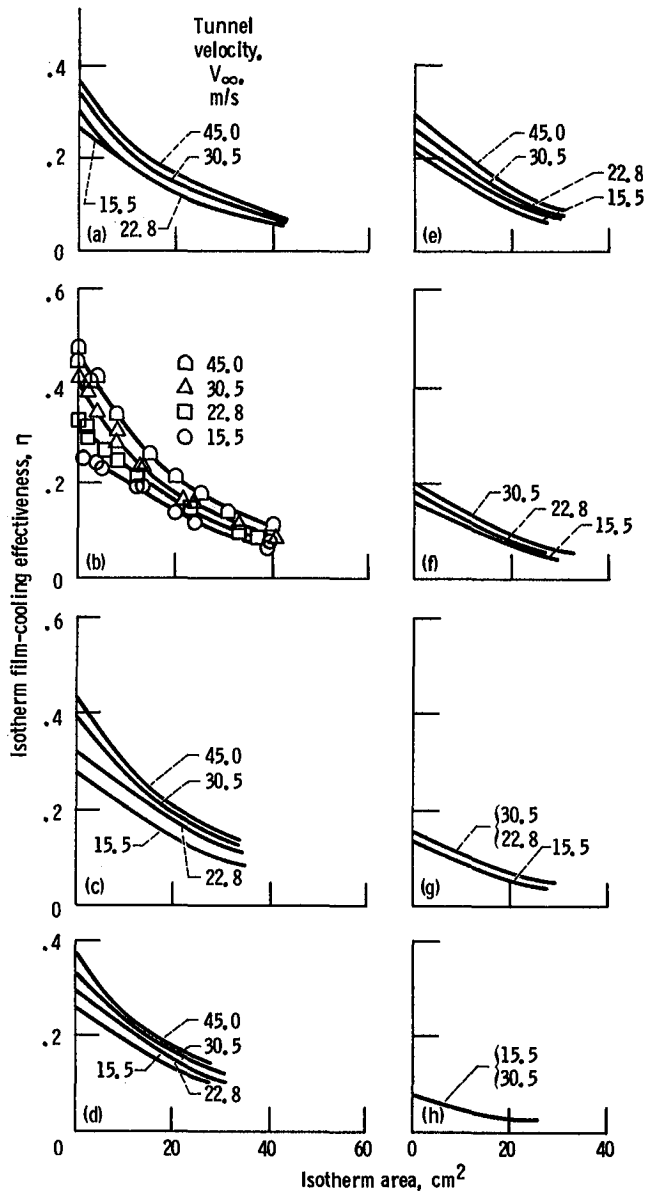
Figure 16.—Basic round hole film-cooling coverage data.
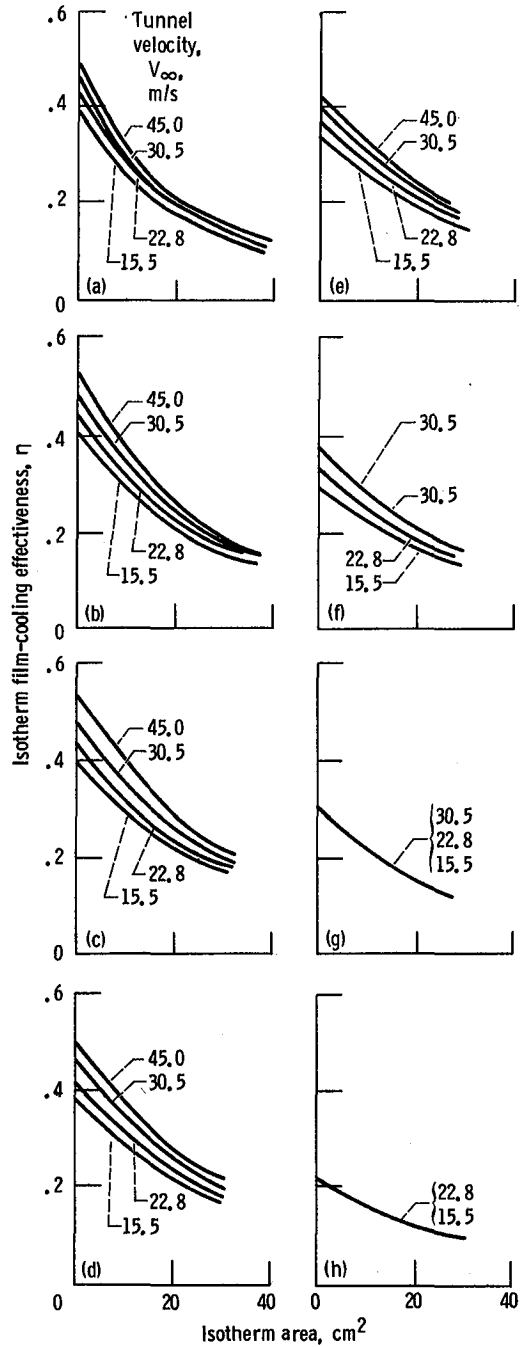
(a) $M = 0.20.$ (e) $M = 1.00.$
(b) $M = 0.34.$ (f) $M = 1.25.$
(c) $M = 0.50.$ (g) $M = 1.50.$
(d) $M = 0.75.$ (h) $M = 2.05.$

Figure 17.—Basic top-cusp film-cooling coverage data.

(a) $M = 0.20.$ (e) $M = 1.00.$
(b) $M = 0.34.$ (f) $M = 1.25.$
(c) $M = 0.50.$ (g) $M = 1.50.$
(d) $M = 0.75.$ (h) $M = 2.05.$

(a) $M = 0.20$. (e) $M = 1.00$.
(b) $M = 0.34$. (f) $M = 1.25$.
(c) $M = 0.50$. (g) $M = 1.50$.
(d) $M = 0.75$. (h) $M = 2.05$.
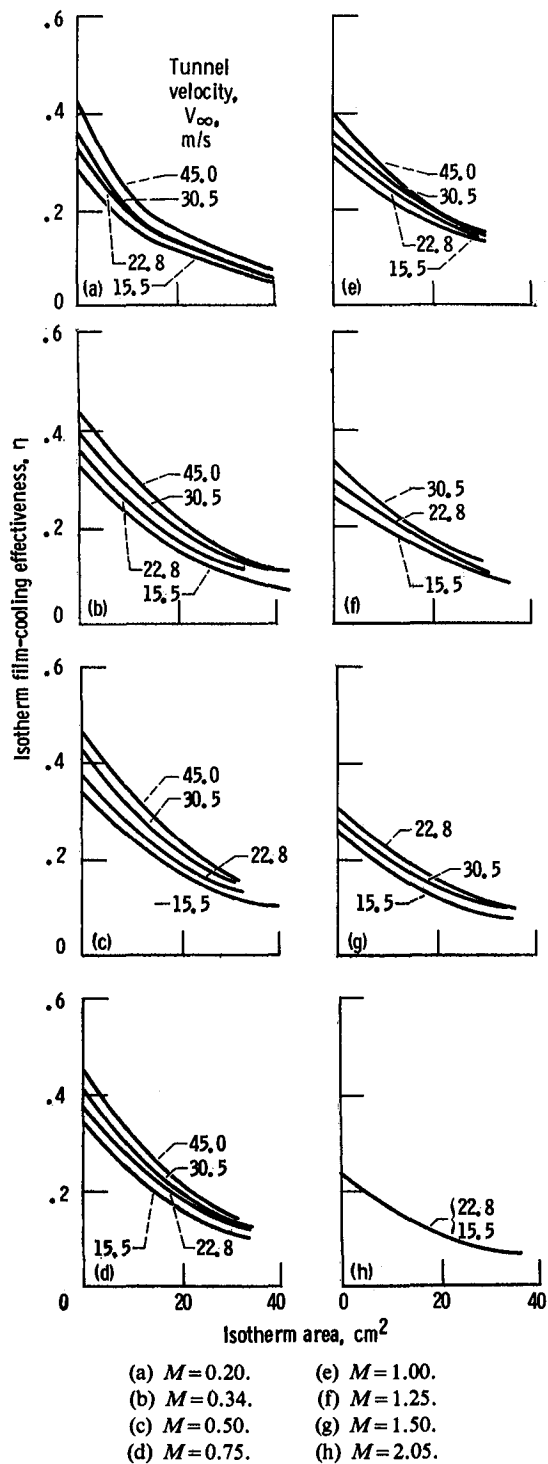
Figure 18.—Basic bottom-cusp film-cooling coverage data.

(a) $M = 0.20$. (e) $M = 1.00$.
(b) $M = 0.34$. (f) $M = 1.25$.
(c) $M = 0.50$. (g) $M = 1.50$.
(d) $M = 0.75$. (h) $M = 2.05$.
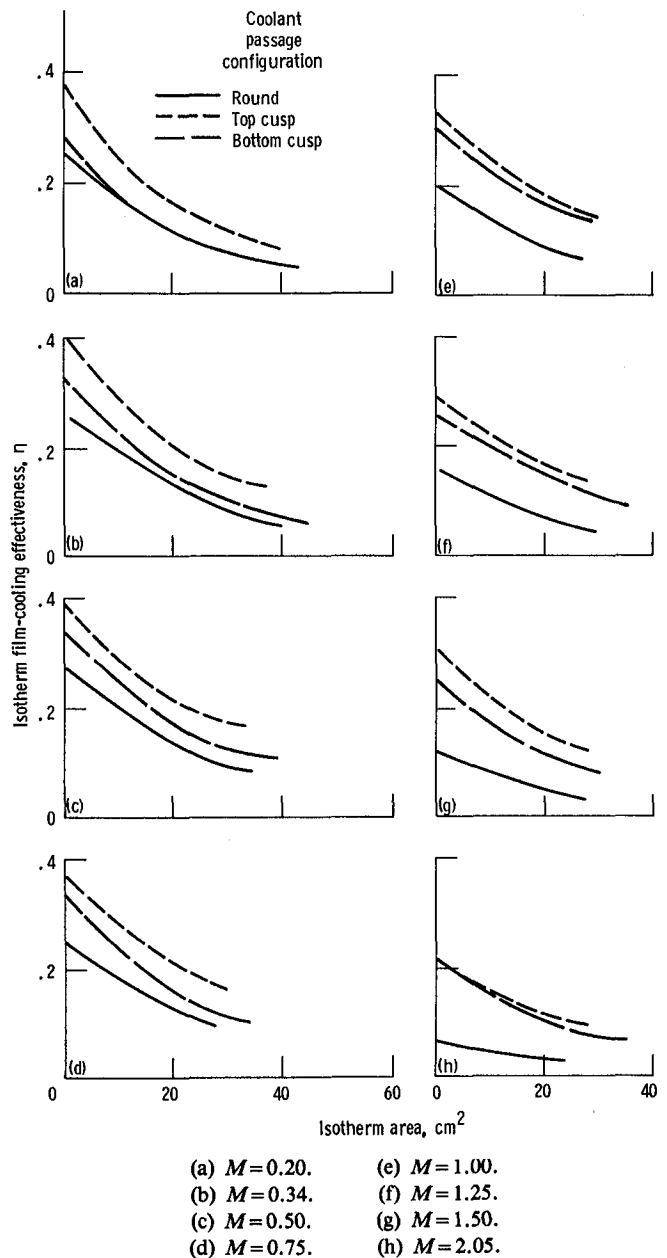
Figure 19.—Film-cooling effectiveness as function of isotherm area for free-stream velocity of 15.5 m/sec.
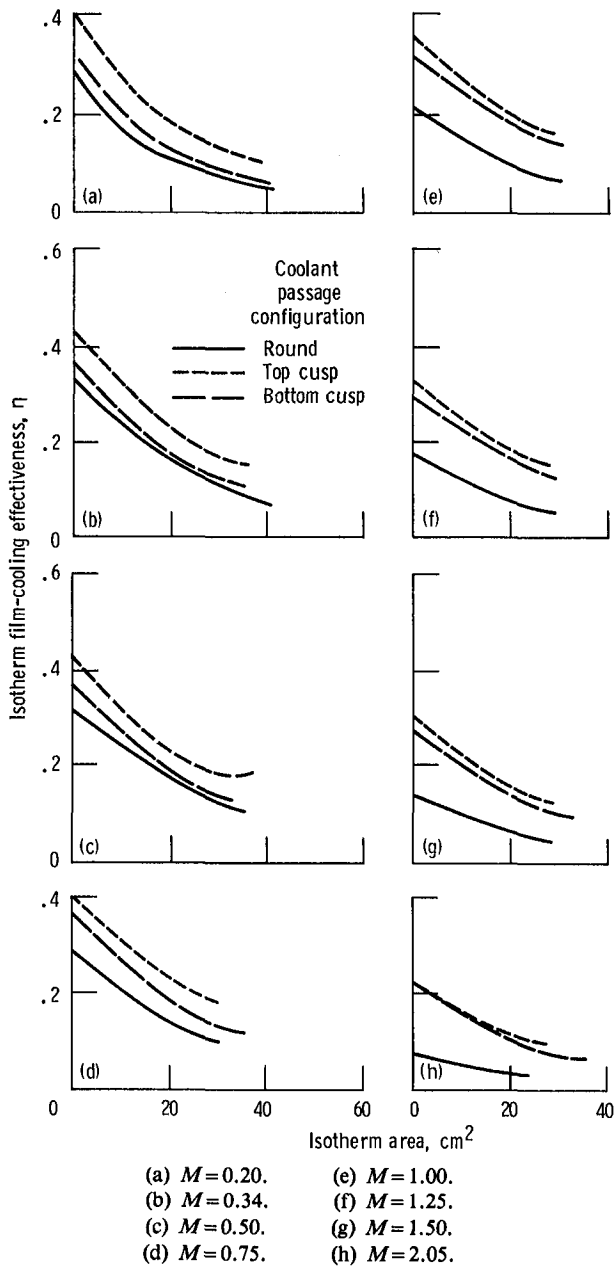
Figure 20.—Comparison of film-cooling coverage data for free-stream velocity of 22.8 m/sec.

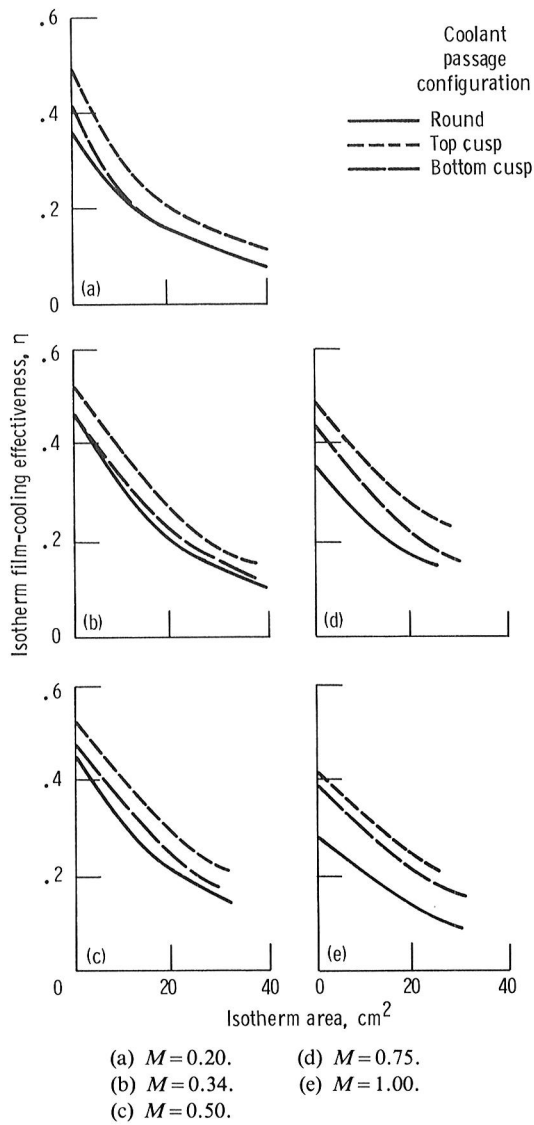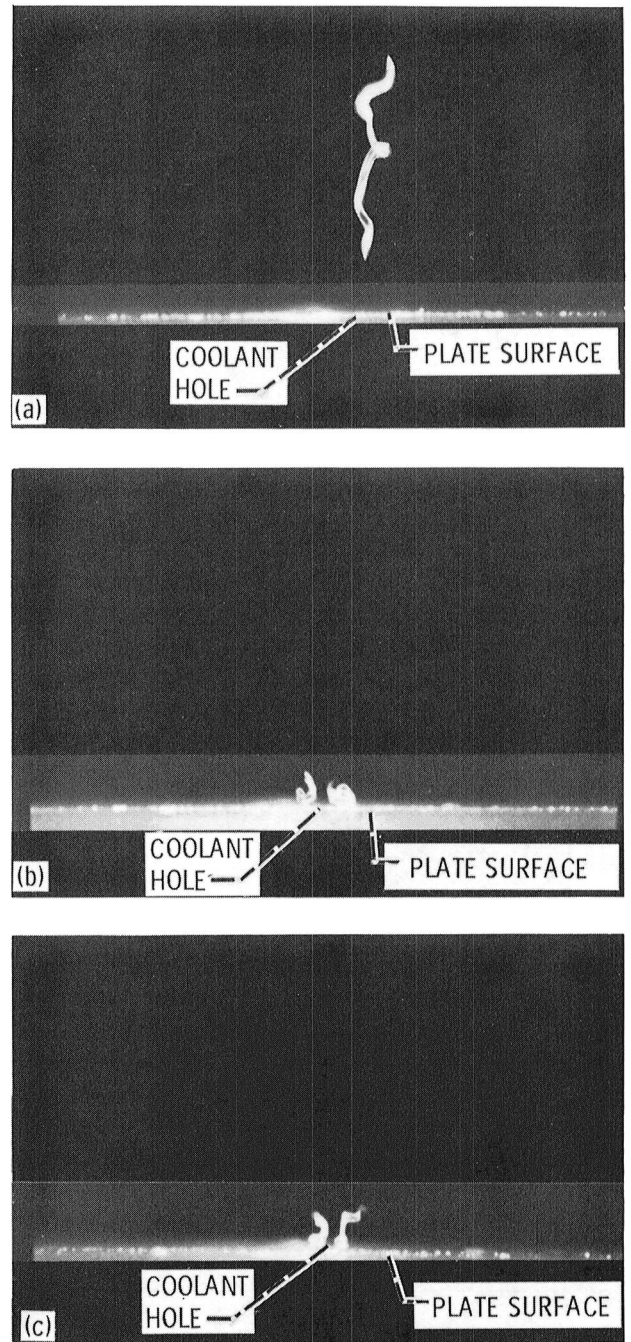(a) $M = 0.20$.   (e) $M = 1.00$.
(b) $M = 0.34$.   (f) $M = 1.25$.
(c) $M = 0.50$.   (g) $M = 1.50$.
(d) $M = 0.75$.   (h) $M = 2.05$.
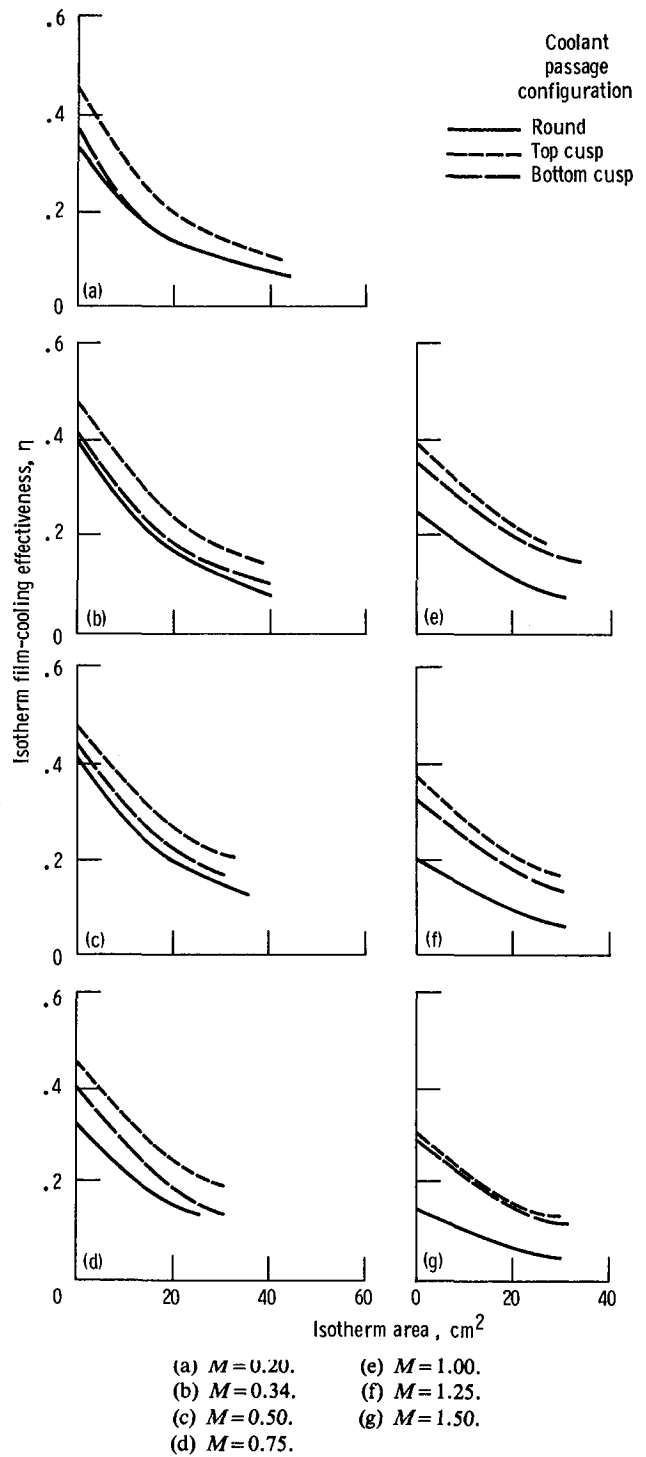
Figure 21.—Comparison of film-cooling coverage data for free-stream velocity of 30.5 m/s.

(a) $M = 0.20$.   (e) $M = 1.00$.
(b) $M = 0.34$.   (f) $M = 1.25$.
(c) $M = 0.50$.   (g) $M = 1.50$.
(d) $M = 0.75$.

(a) $M = 0.20$.   (d) $M = 0.75$.
(b) $M = 0.34$.   (e) $M = 1.00$.
(c) $M = 0.50$.

Figure 22.—Comparison of film-cooling coverage data for free-stream velocity of 45.0 m/s.

(a) Top cusp; tunnel velocity, 0; coolant velocity, 1.6 m/s.
(b) Top cusp; tunnel velocity, 8.7 m/s; coolant velocity, 2.9 m/s; blowing rate, 0.34.
(c) Bottom cusp; tunnel velocity, 15.2 m/s; coolant velocity, 5.0 m/s; blowing rate, 0.34.
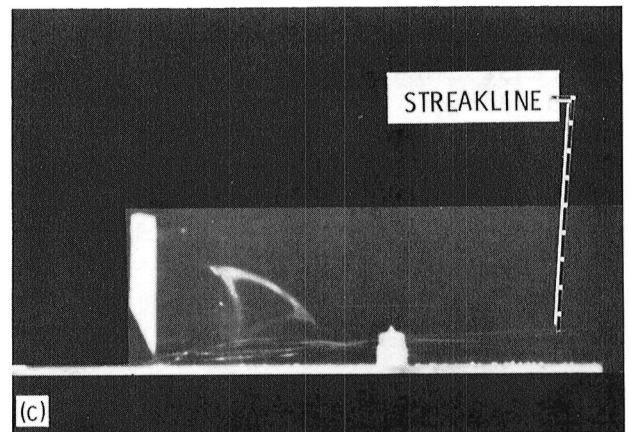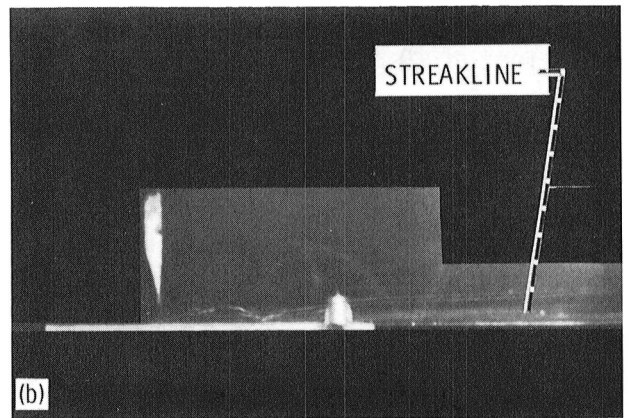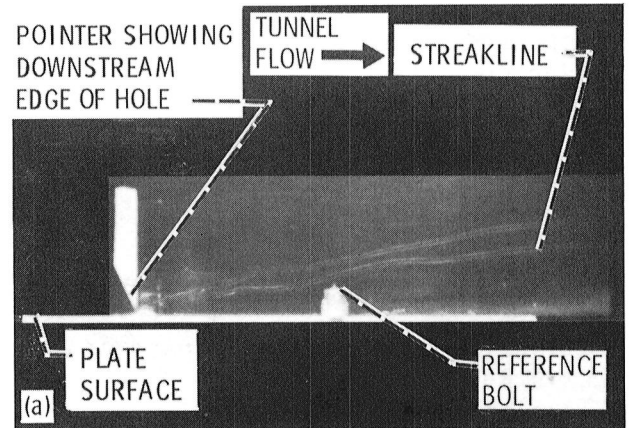
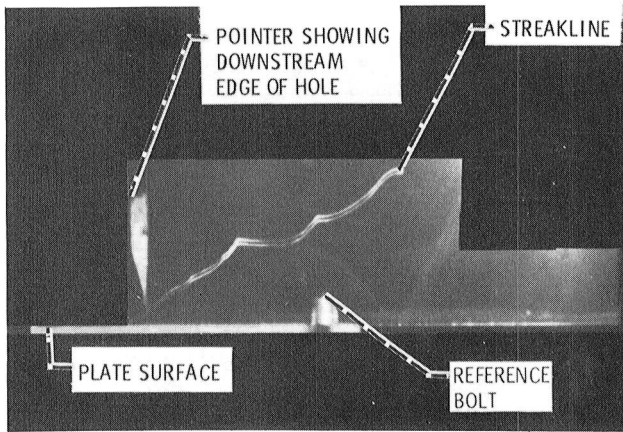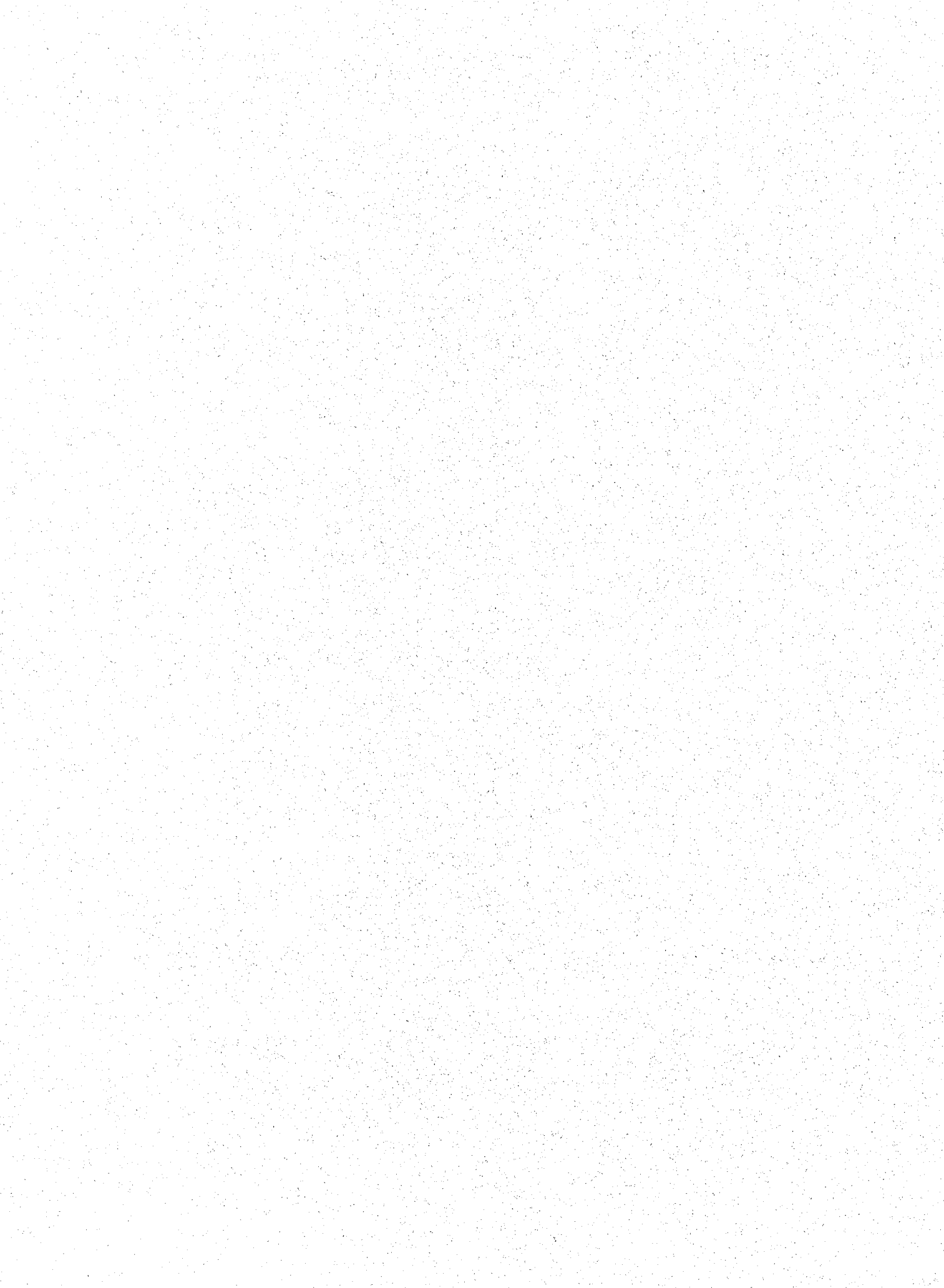Figure 23.—Tunnel view looking downstream.

Figure 24.—Side view of top-cusp configuration. Tunnel velocity, 0; coolant velocity, 7.1 m/s.

(a) Round.
(b) Top cusp.
(c) Bottom cusp.

Figure 25.—Side view. Free-stream velocity, 15.2; coolant velocity, 18.7; blowing rate, 1.25.

1. Report No. NASA TP-2388	2. Government Accession No.	3. Recipient's Catalog No.
4. Title and Subtitle Vortex-Generating Coolant-Flow-Passage Design for Increased Film-Cooling Effectiveness and Surface Coverage		5. Report Date November 1984
		6. Performing Organization Code 505-41-32
7. Author(s) S. Stephen Papell		8. Performing Organization Report No. E-2147
		10. Work Unit No.
9. Performing Organization Name and Address National Aeronautics and Space Administration Lewis Research Center Cleveland, Ohio 44135		11. Contract or Grant No.
		13. Type of Report and Period Covered Technical Paper
12. Sponsoring Agency Name and Address National Aeronautics and Space Administration Washington, D.C. 20546		14. Sponsoring Agency Code

15. Supplementary Notes

16. Abstract

Reported herein are the thermal film-cooling footprints observed by infrared imagery for three coolant-passage configurations embedded in adiabatic-test plates: A standard round-hole cross section and two orientations of a vortex-generating flow passage. Both orientations showed up to factors of four increases in both film-cooling effectiveness and surface coverage over that obtained with the round coolant passage. The crossflow data covered a range of tunnel velocities from 15.5 to 45 m/sec with blowing rates from 0.20 to 2.05. A photographic streakline flow visualization technique supported the concept of the counterrotating capability of the flow passage design and gave visual credence to its role in inhibiting flow separation.

17. Key Words (Suggested by Author(s)) Film cooling Vortex Heat transfer Fluid mechanics Turbine cooling	18. Distribution Statement Unclassified - unlimited STAR category 34		
19. Security Classif. (of this report) Unclassified	20. Security Classif. (of this page) Unclassified	21. No. of pages 22	22. Price* A02

THIRD-CLASS BULK RATE

LANGLEY RESEARCH CENTER

3 1176 01326 5898

U.S.MAIL

NASA

DO NOT REMOVE SLIP FROM MATERIAL

Delete your name from this slip when returning material
to the library.

NAME	DATE	MS
A. Demuren	3/9/	132

NASA Langley (Rev. Dec. 1991)   RIAD N-75